Gelation Mechanism of Poly(*N*-isopropylacrylamide)−Clay Nanocomposite Gels

Sho Miyazaki,[†] Hitoshi Endo,[†] Takeshi Karino,[†,‡] Kazutoshi Haraguchi,[§] and Mitsuhiro Shibayama*[,†,‡]

Neutron Science Laboratory, Institute for Solid State Physics, University of Tokyo, Tokai, Ibaraki 319-1106, Japan; CREST, Japan Science and Technology Agency, 4-1-8 Honcho Kawaguchi, Saitama 332-0012, Japan; and Kawamura Institute of Chemical Research, 631 Sakada, Sakura-shi, Chiba 285-0078, Japan

Received January 15, 2007; Revised Manuscript Received March 19, 2007

ABSTRACT: The gelation mechanism of poly(*N*-isopropylacrylamide)−clay nanocomposite gels (NC gel) was investigated by dynamic light scattering (DLS) and contrast variation small-angle neutron scattering (SANS). It was found that the gelation mechanism of NC gels is similar to that of conventional gels made with organic cross-linker (OR gels). Namely, time-resolved DLS measurements captured all of the characteristic features of gelation at the threshold. This indicates that the gelation of NC gels is also classified to an ergode−nonergode transition. However, the size of the clusters at the gelation threshold is much larger than that of OR gels. This results in a significant depression of optical transmittance exclusively at the gelation threshold for NC gels. Partial scattering functions, i.e., two self-terms $S_{PP}(q)$ and $S_{CC}(q)$ and the corresponding cross-term $S_{CP}(q)$, were obtained by contrast-variation SANS, where P and C denote polymer and clay, respectively, and q is the magnitude of the scattering vector. The detailed analysis of $S_{PP}(q)$, $S_{CC}(q)$, and $S_{CP}(q)$ indicates that (i) each clay platelet is surrounded by polymer layers, (ii) the volume fraction of the polymer layer per clay platelet is independent of the concentrations, and (iii) the correlation length of the network polymer decreases with increasing clay concentration. These results confirm that the screening length of the system is influenced by the concentrations of clay platelets as well as of polymer chains, and the local structures of polymers near clay platelets are similar between in a sol state near the gelation threshold and in bulk NC gels.

Introduction

In recent years, polymer−clay nanocomposite materials attract more and more attention because of their high mechanical properties.[1,2] Recently, Haraguchi et al. developed novel polymer−clay nanocomposite gels (hereafter we call NC gel), which have very large deformability, amazing toughness, high optical transparency, and so on.[3−7] It consists of poly(*N*-isopropylacrylamide) (PNIPA) and the synthetic clay Laponite. In the previous papers, we investigated (i) the microscopic structure of NC gels by dynamic light scattering (DLS) and by small-angle neutron scattering (SANS),[8] (ii) the deformation mechanism under uniaxial stretching,[9] and (iii) its clay concentration dependence by contrast-matched SANS.[10] It was concluded that clay platelets disperse homogeneously in PNIPA matrix and act as multiple cross-linkers. The polymer chains between neighboring "cross-linkers" are much longer than those in conventional chemical gels cross-linked with organic cross-linkers (OR gels), such as methylenebis(acrylamide) (BIS). Interestingly, NC gels can recover their original size after large deformation more than 10 times.[3,11] This indicates that network chains are strongly bound to clay platelets in NC gels. Similar results were obtained by Nie et al.[12−14] In the case of aqueous solutions of a mixture of clay and poly(ethylene oxide) (PEO), there is attractive interaction between clay and PEO. As a result, the solutions behave as physical gels.[15−17] It is clear from a comparison of clay−PEO gels and NC gels the polymer chains in NC gel seem to be strongly anchored to the clay platelets. However, its binding mechanism has not been clarified yet.

For industrial application of NC gels, it is important to understand their gelation mechanisms. Haraguchi et al. investigated the rheological properties of pregel solutions of NC gel.[6] They reported that the viscosity of aqueous solutions of clay decreased by adding *N*-isopropylacrylamide (NIPA) monomer. This is due to shielding of the electric interactions between clay platelets by intercalation of NIPA monomer. They also reported that the optical transmittance depresses sharply during a short period of time in the course of polymerization process. Figure 1 shows the time course of transmittance of an NC gel with $C_{clay} = 0.01$ M and $C_{NIPA} = 1.0$ M (NC1−M1) and OR gel ($C_{NIPA} = 1.0$ M, $C_{BIS} = 0.01$ M) during the polymerization process, where C_{clay} and C_{NIPA} are the concentrations of clay and NIPA, respectively.[6] The transmittance showed a pulselike depression by more than 60% at the polymerization time of ca. 50 min and recovered at 65 min and later. Though the time at the minimum transmittance in this result is later than that as reported by Haraguchi et al.,[6] the phenomenon is the same. Note that such behavior did not appear in the polymerization of OR gels. According to this experimental result, they concluded that the decrease of transmittance was caused by formation of "clay−brush particles" at the beginning of polymerization. However, this phenomenon has not been fully understood. Since it was difficult to terminate the radical chain reaction during the course of polymerization, investigation of the structure and dynamics at the time of the pulselike depression was experimentally unfeasible. In order to elucidate the gelation mechanism of NC gels, particularly by focusing on this suppression, we prepared samples with lower concentrations near the gelation-threshold concentration and investigated the gelation mechanisms of NC

* To whom correspondence should be addressed. E-mail: shibayama@issp.u-tokyo.ac.jp.
[†] University of Tokyo.
[‡] CREST, Japan Science and Technology Agency.
[§] Kawamura Institute of Chemical Research.

10.1021/ma070104v CCC: $37.00
Published on Web 05/08/2007

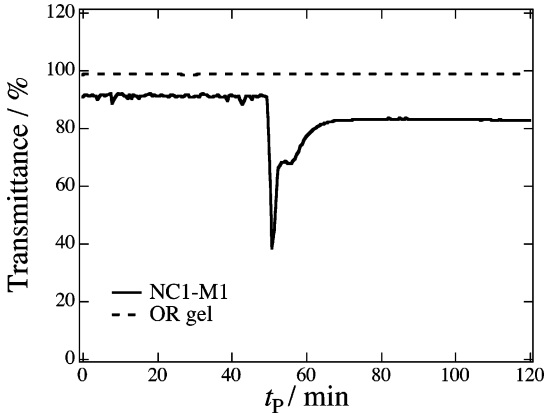

Figure 1. Polymerization time, t_P, dependence of optical transmittance during polymerization for NC gel (NC1−M1) and OR gel.

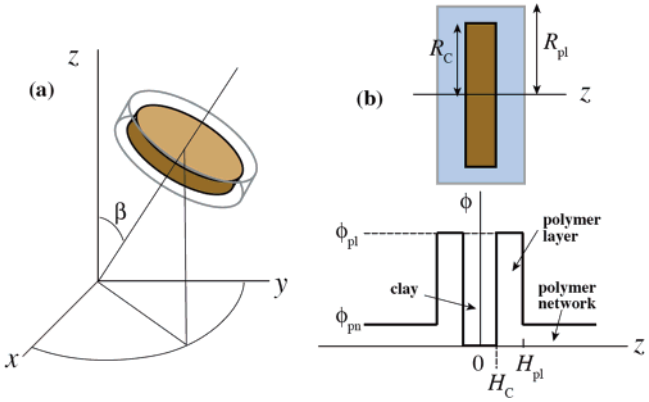

Figure 2. (a) Cartesian coordinate for a randomly oriented cylindrical object with respect to the preferential axis *z*. (b) Decorated clay platelet model sandwiched by polymer layer; the cross-section model (upper) and the polymer concentration profile along *z* axis.

gels from the aspects of structure analyses by means of DLS and contrast-variation SANS.

Theoretical Background

1. DLS Measurement of Gelation Mechanisms. The gelation mechanism of a chemical gel can be investigated by DLS.[18−20] Performing time-resolved DLS, the scattering intensity at the polymerization time t_P at the scattering vector q, $I(t_P;q)$, increases steeply at the gelation threshold. The intensity−time correlation function $g^{(2)}(\tau;t_P;q)$ defined by

$$g^{(2)}(\tau;t_P;q) = \frac{\langle I(t_P;q)\, I(t_P+\tau;q)\rangle}{\langle I(t_P;q)\rangle^2} \qquad (1)$$

also shows characteristic change at the gelation threshold, namely, (i) the initial value ($\tau \to 0$) of $g^{(2)}(\tau;t_P;q) - 1$ is close to unity in the sol state and far below than unity in the gel state. These correspond to ergodic and nonergodic states, respectively; (ii) $g^{(2)}(\tau;t_P;q) - 1$ changes from a stretched exponential function to a power-law function; and (iii) the characteristic decay rate distribution function $G(\Gamma;t_P)$ becomes broadest. Here, $G(\Gamma;t_P)$ is obtained by inverse Laplace transform using the constrained regularization program CONTIN,[21] as follows:

$$g^{(2)}(\tau;t_P;q) - 1 = [\int_0^\infty G(\Gamma;t_P)\exp(-\Gamma\tau)\,d\Gamma]^2 \qquad (2)$$

where Γ is the characteristic decay rate (an inverse of the characteristic decay time, Γ^{-1}). Here, $G(\Gamma;t_P)$ shows a broad distribution at the time of gelation threshold t_{th}, indicating a fractal-like distribution of clusters. Then it shrinks back to a single peak with a relatively fast decay time (the gel mode) for $t \gg t_{th}$.

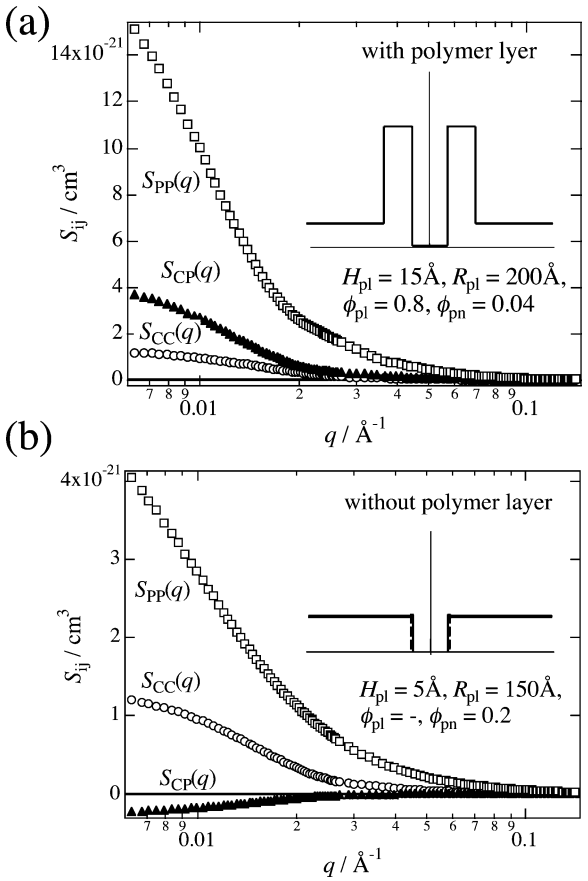

Figure 3. Examples of partial scattering functions, $S_{CC}(q)$, $S_{CP}(q)$, and $S_{PP}(q)$. Note that $S_{CP}(q)$ is (a) positive if there exists a polymer layer and (b) negative if no polymer layer exists.

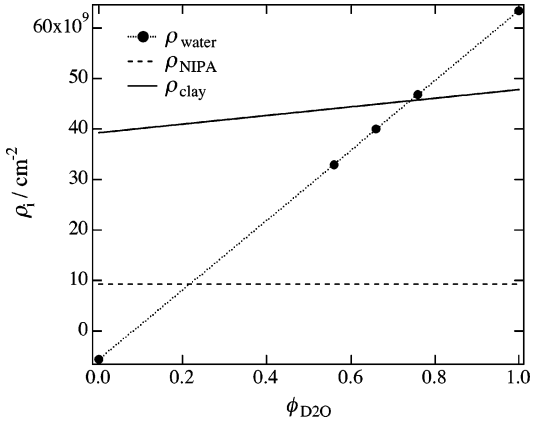

Figure 4. Scattering length densities, ρ_i, of i = water, clay, and PNIPA, as a function of D_2O fraction.

2. SANS Analysis Applying Contrast Variation for Three-Component Systems. In the case of three-component systems, the scattering intensity function is written as follows (on the basis of assumption of incompressibility):

$$I(q) = (\rho_1 - \rho_3)^2 S_{11}(q) + (\rho_2 - \rho_3)^2 S_{22}(q) + 2(\rho_1 - \rho_3)(\rho_2 - \rho_3) S_{12}(q) \qquad (3)$$

Here, ρ_i ($= \sum_j b_j/v_i$) indicates the scattering length density of each component, i (i = 1, 2, and 3), and b_j is the scattering

length of *j*th atom and v_i is the volume of the molecule. $S_{ij}(q)$'s are the partial scattering functions. $S_{11}(q)$ and $S_{22}(q)$ are called the self-terms, representing the self-correlations of component 1 and 2, respectively. $S_{12}(q)$ is called the cross-term, representing the cross-correlation between components 1 and 2. Note that $S_{ij}(q)$ is normalized by the absolute intensity and the scattering length density and has a dimension of volume. We performed contrast-variation SANS experiments by tuning the scattering length density of component 3, ρ_3, in order to decompose the scattering intensities into the partial scattering functions as follows:

$$\begin{pmatrix} S_{11}(q) \\ S_{22}(q) \\ S_{12}(q) \end{pmatrix} = \begin{pmatrix} {}^1\Delta\rho_1{}^2 & {}^1\Delta\rho_2{}^2 & 2{}^1\Delta\rho_1{}^1\Delta\rho_2 \\ {}^2\Delta\rho_1{}^2 & {}^2\Delta\rho_2{}^2 & 2{}^2\Delta\rho_1{}^2\Delta\rho_2 \\ \vdots & \vdots & \vdots \\ {}^n\Delta\rho_1{}^2 & {}^n\Delta\rho_2{}^2 & 2{}^n\Delta\rho_1{}^n\Delta\rho_2 \end{pmatrix}^{-1} \begin{pmatrix} I_1(q) \\ I_2(q) \\ \vdots \\ I_n(q) \end{pmatrix} \quad (4)$$

where ${}^m\Delta\rho_i \equiv \rho_i - \rho_3$ is the difference of the scattering length densities between components *i* and 3 of the *m*th measurement. The transposed matrix of contrast matrix, ${}^T({}^{m\times n}\Delta\rho)$, which fulfills the condition ${}^T({}^{m\times n}\Delta\rho)\cdot({}^{m\times n}\Delta\rho) = E$, can be obtained by *singular value decomposition*. The detailed description of the procedure can be found elsewhere.[22]

Hereinafter, we calculate the scattering functions for NC gels. NC gel consists of three components, i.e., clay, PNIPA, and solvent. Let us assume a cylindrical scattering object, as shown in Figure 2a, of which the preferential axis is randomly oriented with respect to the *z*-axis with the azimuthal angle of β. The scattering amplitude for a cylindrical clay platelet schematically drawn in Figure 2b reads as

$$A_{cyl}(R,H,\beta) = 2V\frac{\sin(qH\cos\beta)}{qH\cos\beta}\frac{J_1(qR\sin\beta)}{qR\sin\beta} \quad (5)$$

where V is the volume of the cylinder, $V = \pi R^2 2H$, and $J_1(x)$ is the Bessel function of the first kind. According to the Appendix, one obtains the partial structure factors as follows:

$$S_{CC} = \frac{n_C}{2}\int_{\beta=0}^{\pi} A_{cyl}(R_C,H_C,\beta)^2 \sin\beta\, d\beta \quad (6)$$

$$S_{CP} = \frac{n_C}{2}(\phi_{pl} - \phi_{pn})\int_{\beta=0}^{\pi} A_{cyl}(R_C,H_C,\beta)\, A_{cyl}(R_{pl},H_{pl},\beta)\sin\beta\, d\beta - \frac{n_C}{2}\phi_{pl}\int_{\beta=0}^{\pi} A_{cyl}{}^2(R_C,H_C,\beta)\sin\beta\, d\beta \quad (7)$$

$$S_{PP} = \frac{n_C}{2}\int_{\beta=0}^{\pi}[(\phi_{pl} - \phi_{pn})A_{cyl}(R_{pl},H_{pl},\beta) - \phi_{pl}A_{cyl}(R_C,H_C,\beta)]^2\sin\beta\, d\beta + \frac{S_{PP}^0(0)}{1+\xi^2q^2} \quad (8)$$

where n_C is the number density of clay platelets, and R_C and H_C correspond to the radius and the half-height of clay platelet, respectively. In eqs 7 and 8, ϕ_{pl}, ϕ_{pn}, R_{pl}, and H_{pl} represent the local volume fraction of the polymer layer, the volume fraction of polymer which is not adsorbed to clay platelets, the radius of polymer layer, and the half-height of polymer layer, respectively. The last term of the right-hand side of eq 8 is the Ornstein−Zernike term, representing the polymer network with the correlation length ξ. Here, the cross-correlation of the polymer network and the clay platelet is negligible. However, it becomes significant when the clay concentration is high and/or ξ is comparable with the size of clay platelet. If there is no polymer layer, $R_{pl} = R_C$, $H_{pl} = H_C$, and $S_{CP}(q)$ becomes

$$S_{CP}(q) = -\phi_{pn}S_{CC}(q) \quad (9)$$

Figure 3 shows examples for numerical calculation of the partial scattering functions (a) with and (b) without clay−polymer cross-correlation. Here, we substituted $R_C = 150$ Å, $H_C = 5$ Å, $\xi = 100$ Å, and (R_{pl}, H_{pl}, ϕ_{pl}, ϕ_{pn}) = (200 Å, 15 Å, 0.8, 0.04) for (a) as well as (150 Å, 5 Å, −, 0.2) for (b). These parameters are chosen so as to make it clear the difference between the two cases. It is worth noting that the sign of $S_{CP}(q)$ is positive in the case with correlation and negative without correlation. From the sign of $S_{CP}(q)$, we can learn whether there is cross-correlation between clay and polymer or not. A "contrast matching" experiment allows one to obtain only the self-terms, but not the cross-terms. By conducting "contrast variation" analysis, on the other hand, we can directly access the cross-correlation between the two different components.

Experimental Section

Samples. NC gel is obtained by free radical polymerization of *N*-isopropylacrylamide (NIPA) monomer in the presence of the synthetic clay Laponite XLG ($[Mg_{5.34}Li_{0.66}Si_8O_{20}(OH)_4]Na_{0.66}$). We used potassium peroxodisulfate (KPS) and *N*,*N*,*N*′,*N*′-tetramethylethylenediamine (TEMED) as an initiator and a catalyst, respectively. Since the polymerization completes in a very short period of time, it is difficult to investigate the gelation mechanism by an in-situ SANS measurement. Therefore, we prepared NC gels of four different concentrations by keeping the constant ratio of PNIPA to clay for DLS measurements as well as contrast variation SANS. The sample codes were defined by the concentrations (C_{clay}/M, $C_{monomer}$/M) of the clay and NIPA monomer, i.e., NC1−M0.4, NC0.6−M0.24, NC0.2−M0.08, and NC0.05−M0.02. They indicate that the combinations of the molar concentrations were (C_{clay}/M, $C_{monomer}$/M) = (0.01, 0.4), (0.006, 0.24), (0.002, 0.08), and (0.0005, 0.02), respectively. Note that NC0.2−M0.08 and NC0.05−M0.02 remained in the sol state and NC1−M0.4 and NC0.6−M0.24 became gels after polymerization.

DLS. DLS measurements were performed by a static/dynamic compact goniometer (DLS/SLS-5000), ALV, Langen, Germany. A He−Ne laser with a power of 22 mW emitting a polarized light at $\lambda = 6328$ Å was used as the incident beam. DLS measurements were taken at 20 °C at scattering angles of 30°−150°. For time-resolved DLS measurements, average intensities were collected with an interval of 30 s for 2 h during the reaction. The samples for DLS experiments were prepared in a test tube under nitrogen purge. For comparison, a conventional PNIPA gel cross-linked with *N*,*N*′-methylenebis(acrylamide) (BIS) OR gel with $C_{NIPA} = 1.0$ M and $C_{BIS} = 0.01$ M was also prepared.

SANS. SANS experiments were performed at the SANS instrument (SANS-U) of Institute for Solid State Physics, The University of Tokyo.[24] The neutron wavelength was 7.0 Å, and its distribution was ca. 10%. The sample-to-detector distance was chosen to be 2 and 8 m, and the q range was from 0.005 to 0.15 Å^{-1}. The necessary corrections were made, such as air scattering, cell scattering, and incoherent background subtraction.[25] After these corrections, the scattered intensity was normalized to the absolute intensity in terms of the scattering intensity from a standard sample. The temperature of the samples was regulated to be 20 °C with a water-circulating bath controlled with a Neslab RTE-111 thermocontroller with the precision of ±0.1 °C.

For contrast-variation SANS, a series of samples with different scattering length densities of solvent were prepared. The scattering length densities were calculated on the basis of their chemical structures and mass densities. The used mass densities are 2.65 g/cm^3 for the clay, 1.26 g/cm^3 for NIPA, and 1.00 g/cm^3 for the aqueous solvent. Figure 4 shows the scattering

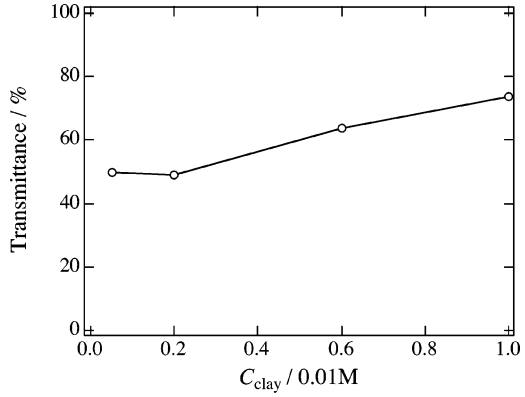

Figure 5. C_{NIPA} dependence of optical transmittance for NC gels near the gelation threshold.

length densities of each component as a function of the volume fractions of D_2O, ϕ_{D_2O}. The contrast variations were performed with $\phi_{D_2O} = 0$, 0.56, 0.66, 0.76, and 1.0, which were marked by filled circles on the line of the scattering length density of water in the figure. The scattering length density of water varies with ϕ_{D_2O}. Hydrogen/deuterium exchange should be also taken into account for clay. Hence, in general, the scattering length density of component i with H/D replacement, $\rho_i(\phi_{D_2O})$, is given as a function of ϕ_{D_2O} by

$$\rho_i(\phi_{D_2O}) = \phi_{D_2O}\rho_{i,D} + (1 - \phi_{D_2O})\rho_{i,H} \quad (10)$$

where $\rho_{i,D/H}$ is the scattering length density in the pure D_2O/H_2O solvent.

Results and Discussion

1. DLS. Figure 5 shows the optical transmittance for NC0.05−M0.02, NC0.2−M0.08, NC0.6−M0.24, and NC1−M0.4 as a function of C_{clay}. Note that the transmittance is much lower than unity, and these samples represent the situation of NC gels during polymerization shown in Figure 1. Now we investigate the dynamics and microscopic structures of NC gels near gelation threshold by DLS.

Figure 6a shows the time dependence of normalized scattering intensity, I_s/I_0, for NC gel and OR gel with the same C_{NIPA} as a function of the reaction time, t_P. The scattering angle was 90° ($q = 0.0018$ Å^{-1}). All the samples show an abrupt increase at the polymerization time at gelation threshold, $t_P = t_{th}$ ($t_{th} \approx$ 13.6 min for OR gel and $t_{th} \approx 50.9$ min for NC gel). Note that the intensity of NC gel at its peak is much larger than that of OR gel. This suggests that the cluster size of NC gel at the gelation threshold is much larger than that of OR gel. In the case of NC gels, the inter-cross-linker distance is much larger than that of chemical gels, and clay platelets act as plane cross-linkers. This is the reason why large clusters are formed in NC gel at the gelation threshold, followed by percolation transition to a gel. The large clusters scatter the light more strongly than the case of OR gel, resulting in a sharp dip in the transmittance. Figure 6b shows $g^{(2)}(\tau;t_P;q) - 1$ of NC1−M1 at $q = 0.0018$ Å^{-1}. As shown in the figure, profiles (1) and (2) have characteristic relaxation modes around $\tau \approx 0.50$ ms for $t_P < t_{th}$. Polymerization reaction did not start for $t_P < t_{th}$. However, once polymerization starts (3), it steeply shifts to a larger τ. At $t_P \approx t_{th}$, a power-law behavior appears in $g^{(2)}(\tau;t_P;q) - 1$, indicating a fractal-like distribution of clusters (4). Then a gel mode appeared for $t_P \gg t_{th}$, (5) and (6).

Figure 7 shows the results of DLS measurements for NC0.05−M0.02, NC0.2−M0.08, NC0.6−M0.24, and NC1−M0.4 after completion of polymerization. Figure 7a shows the

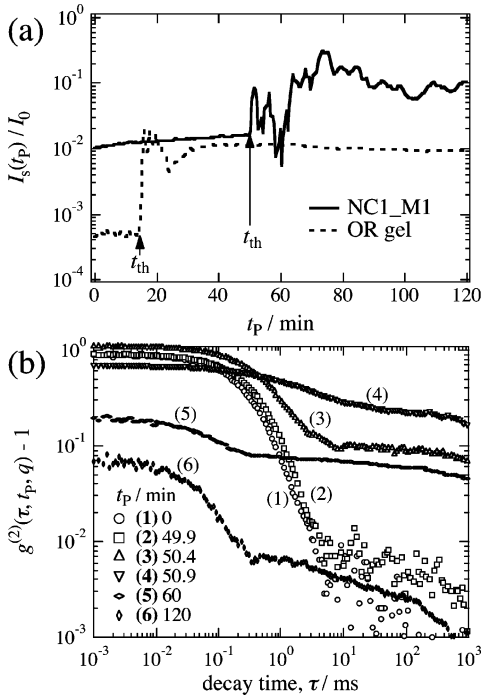

Figure 6. (a) Polymerization time dependence of the scattering intensity, $I_s(t_P)/I_0$, for NC gel and OR gel. (b) Series of time−intensity correlation functions of NC gel (NC1−M1) at various t_P's.

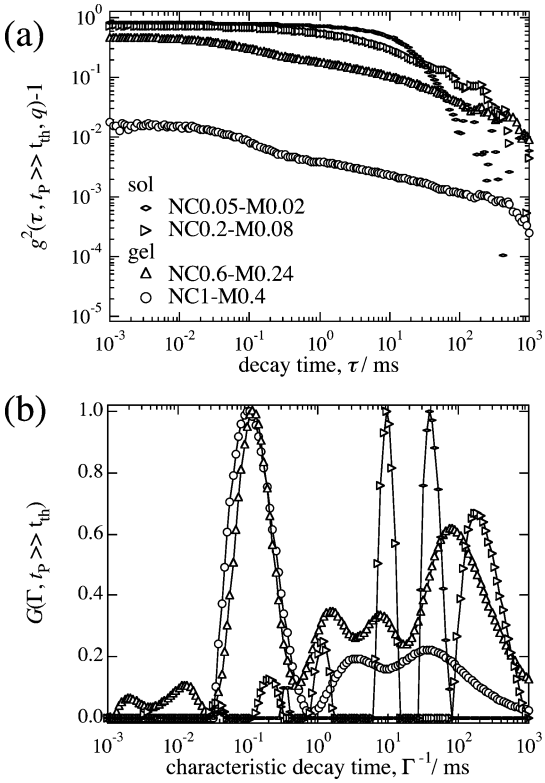

Figure 7. DLS results of NC gels near the gelation threshold: (a) time−intensity functions and (b) the distribution functions $G(\Gamma;t_P \gg t_{th})$.

intensity−time correlation functions, $g^{(2)}(\tau;t_P \gg t_{th};q) - 1$, as a function of τ, and Figure 7b shows the characteristic decay time distribution functions, $G(\Gamma;t_P \gg t_{th})$. NC0.05−M0.02 and NC0.2−M0.08 are in sol state because of $g^{(2)}(\tau=0;t_P \gg t_{th};q) - 1 \approx 1$. On the other hand, the initial values of $g^{(2)}(\tau;t_P;q) - 1$ for NC1−M0.4 and NC0.6−M0.24 are less than unity, indicating that these are in gel state and in nonergodic. Because of nonergodicity, we obtained correlation functions at 10 different sample

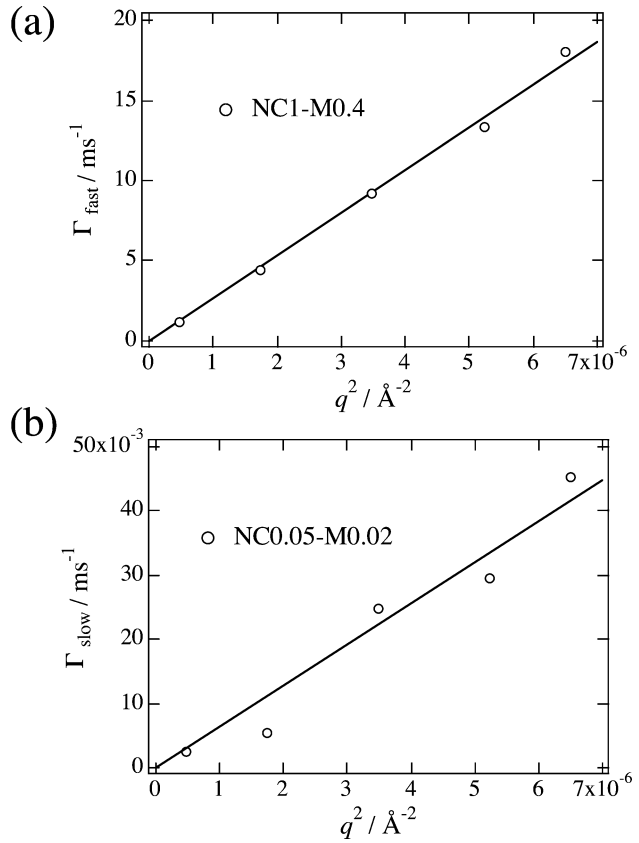

Figure 8. q dependence of the characteristic decay rates of (a) the fast mode, Γ_{fast} (NC1−M0.4), and (b) the slow mode Γ_{slow} (NC0.05−M0.02).

positions for the gels. The curves of $G(\Gamma;t_P \gg t_{th})$ for the gels in Figure 7b are representative one without loss of generality. The distribution functions of these two samples have a peak around 0.1 ms. This peak corresponds to the so-called gel-mode. The mesh size is estimated to be ca. 53 Å. Note that both samples have another broad distribution mode. This indicates that finite clusters are still present in the system at these concentrations. This is due to that the reaction completed before gelation threshold and finite clusters; i.e., "microgels" are formed. Such a broad distribution is not observed in well-grown NC gels with higher C_{clay} and C_{NIPA}.[8] $g^{(2)}(\tau;t_P;q) - 1$of NC0.6−M0.24 shows a power-law-like behavior in the region for $\tau > 0.1$ ms, indicating that this sample is very close to the gelation threshold. $g^{(2)}(\tau;t_P;q) - 1$ of NC0.05−M0.02 shows a single-exponential decay at a very large τ, i.e., $\tau \approx 38$ ms. The hydrodynamic radius calculated from the Einstein−Stokes equation was about 3.0×10^4 Å. Because NC0.05−M0.02 remains in sol state near the sol−gel transition point after the completion of the reaction, this value is an estimate of the largest cluster size for NC0.05−M0.02. Since this size is comparable to the wavelength of visible light, the NC gels at these concentrations scatter light, resulting in a depression of transmittance.

Figure 8 shows the scattering angle dependence of the characteristic decay rates, Γ_{fast} (=Γ_{gel}; the gel mode) for NC1−M0.4 and Γ_{slow} for NC0.05−M0.02 (the translational mode of large clusters). As shown in the figure, the decay rates are proportional to q^{-2}. This indicates that both modes are diffusive. According to these results, the gelation mechanism of NC gel is similar to that of chemical gel. That is, clusters are formed after an initiation of polymerization, and they grow up until they reach percolation threshold, followed by maturing as a bulk gel. The difference between the two types of gels lies in the

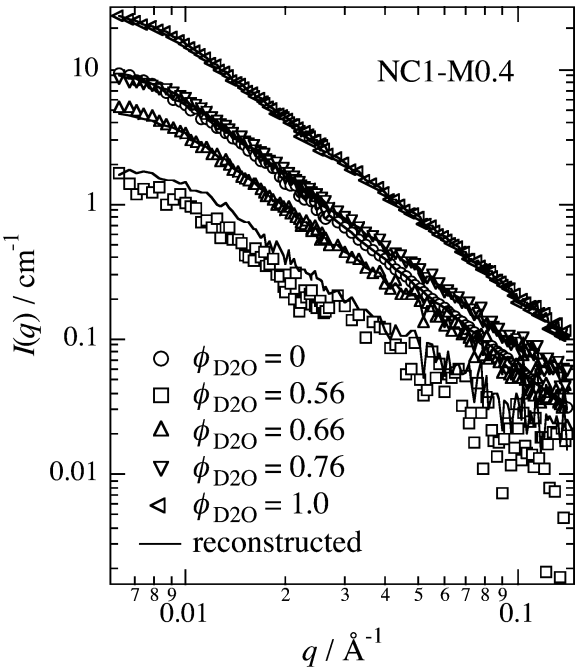

Figure 9. Results of contrast-variation SANS for NC1−M0.4. The solid lines are the reconstructed scattering intensity functions from decomposed partial scattering functions.

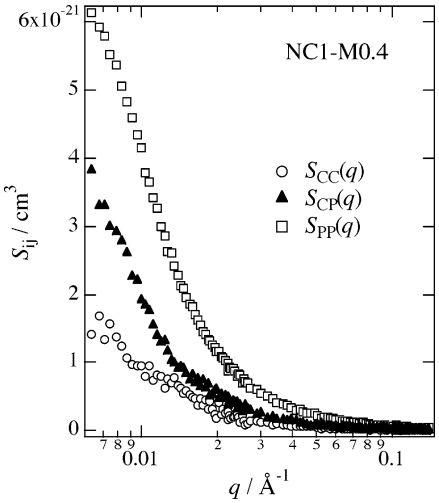

Figure 10. Partial scattering functions of the clay−clay $S_{CC}(q)$, the clay−polymer cross-term $S_{CP}(q)$, and the polymer−polymer $S_{PP}(q)$, decomposed from $I(q)$'s in Figure 9.

size of finite clusters near the gelation threshold. The clusters in NC gels are much larger than those in OR gels. Now we will investigate the microscopic structure by contrast variation SANS.

2. SANS. Figure 9 shows the absolute scattering intensity functions, $I(q)$, of NC1−M0.4 with solvents of different D_2O fractions. The shapes of $I(q)$'s were quite similar. Note that $I(q)$ of $\phi_{D_2O} = 0$ is larger than that of $\phi_{D_2O} = 0.56$. $I(q)$ becomes larger with increasing ϕ_{D_2O} for $\phi_{D_2O} > 0.56$. The scattering length density of the solvent is matched with that of clay at $\phi_{D_2O} = 0.75$. However, it is interesting to note that $I(q)$ is not the minimum at $\phi_{D_2O} = 0.75$. $I(q)$'s of the other three ϕ_{D_2O}'s change in a similar fashion. This indicates that the contribution to $I(q)$ from PNIPA is larger than that of clay.

$I(q)$'s of NC gels can be decomposed into partial scattering functions by using singular value decomposition (see eq 4). Figure 10 shows the partial scattering functions, $S_{PP}(q)$, $S_{CC}(q)$, and $S_{CP}(q)$ of NC1−M0.4. From these partial scattering func-

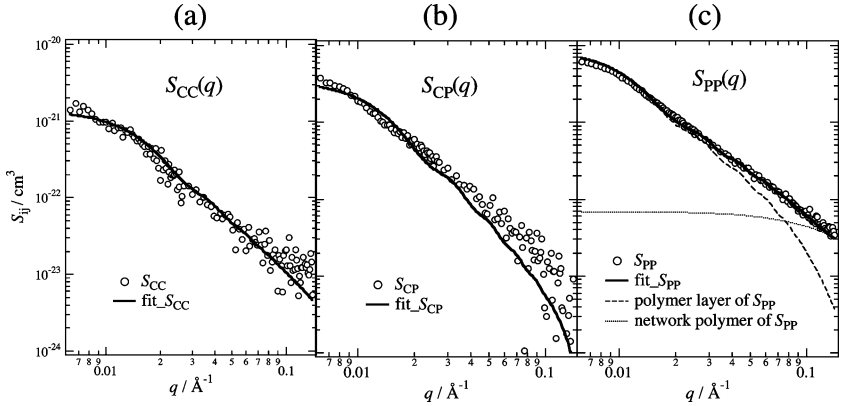

Figure 11. Example of partial scattering functions and their fitting results with model functions (a) $S_{CC}(q)$, (b) $S_{CP}(q)$, and (c) $S_{PP}(q)$. The dashed line in (c) is obtained by fixing the parameters about polymer layer to the value resulting from $S_{CP}(q)$, and the dotted line shows the contribution of polymer network from fitting. The solid line is the sum of the two terms.

tions, $I(q)$'s of NC gels were well reconstructed by eq 3 (solid line in Figure 9), indicating that the partial scattering functions are obtained with high accuracy. The same applies for the other three samples. As discussed above and shown in Figure 10, $S_{PP}(q)$ is larger than $S_{CC}(q)$. This is because that the volume fraction of PNIPA, ϕ_{NIPA}, is much larger than that of clay, ϕ_{clay}. The most remarkable result was that the cross-term $S_{CP}(q)$ is positive and between $S_{CC}(q)$ and $S_{PP}(q)$. As discussed in the theoretical section, the behavior of $S_{CP}(q)$ is quite meaningful because $S_{CP}(q)$ tells the correlation between clay and polymer chains. The fact that $S_{CP}(q)$ is in between $S_{CC}(q)$ and $S_{PP}(q)$ suggests the following. There is noticeable spatial cross-correlation between PNIPA and clay. If there is no or little cross-correlation between them, $S_{CP}(q)$ should be negative for all or wide range of q. This argument leads to the following hypothesis. The clay platelets are surrounded by polymer layer, where local volume fraction of PNIPA is higher than that of the bulk gel. Since PNIPA chains and clay surface have attractive interaction, this hypothesis seems to be reasonable. As a more concrete picture, dangling PNIPA chains may be captured to the clay surface by the attractive interaction and make dense polymer layer. The network chains anchored to the clay platelets are assumed to have no cross-correlation with clay. From this model, partial scattering functions $S_{CC}(q)$, $S_{CP}(q)$, and $S_{PP}(q)$ are obtained by eqs 6, 7, and 8, respectively.

Figure 11 shows the fitting result of (a) $S_{CC}(q)$, (b) $S_{CP}(q)$, and (c) $S_{PP}(q)$ of NC1−M0.4. $S_{CC}(q)$ was well represented by the scattering function of thin disk with the value of literature and the number density of clay calculated from concentration, i.e., 150 Å height, 10 Å thickness, and 2.80×10^{15} cm^{-3} number density. From the fitting of $S_{CP}(q)$, the size and the local concentration of the polymer layer are estimated to be about 200 Å in radius and about 30 Å in height and about 60 vol %, respectively. $S_{PP}(q)$ is further decomposed into two contributions, i.e., the scattering from polymer network represented by OZ function (solid line) and the polymer layer (dotted line). The thick line is the sum of these two contribution, which again well represents $S_{PP}(q)$.

SANS measurements were also performed to NC0.6−M0.24, NC0.2−M0.08, and NC0.05−M0.02 and were decomposed into the partial scattering functions. Similarly to the NC1−M0.4, its cross-term, $S_{CP}(q)$, was positive and in between $S_{CC}(q)$ and $S_{PP}(q)$. Then we analyzed them with the same model. According to the fitting results, the thickness and the local concentration of the polymer layer was found to be almost the same, and the correlation length of the polymer network is larger than that of NC1−M0.4.

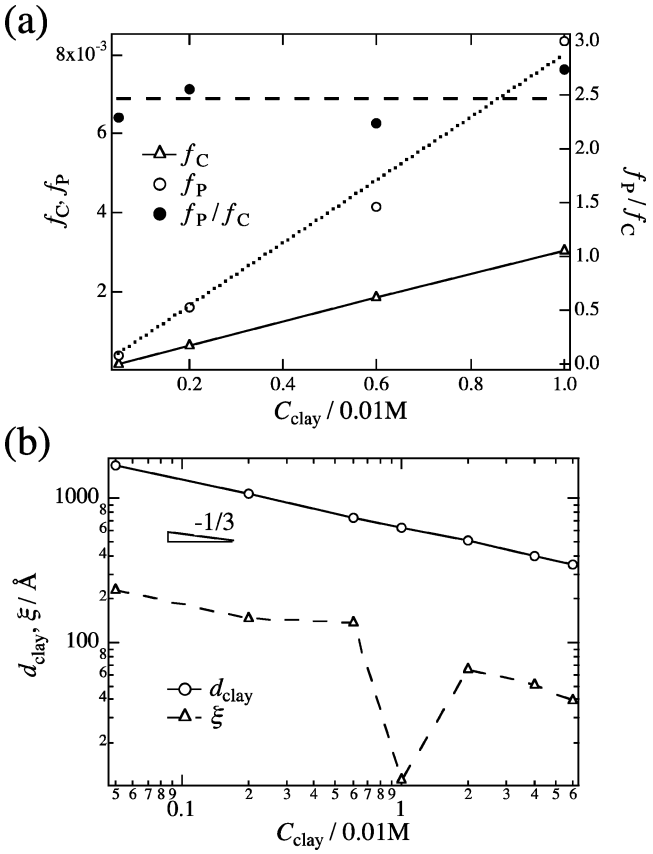

Figure 12. (a) Clay concentration C_{clay} dependence of the fraction of space occupied by polymer layer (f_{pl}; dotted line) and by clay (f_{clay}; solid line). The thick-dashed line indicates the ratio of f_{pl}/f_{clay}. (b) C_{clay} dependence of the interclay distance, d_{clay}, and the correlation length, ξ.

Figure 12a shows the C_{clay} dependence of the fitting results related to the polymer layer. The solid line and dotted line represent the volume fractions of the space occupied by clay, f_C, and by the polymer layer, f_{pl}, respectively. Here, f_{pl} is calculated by

$$f_{pl} = \phi_{pl} f_C \frac{V_P - V_C}{V_C} \tag{11}$$

Both f_C and f_{pl} increase with increasing C_{clay}. The thick line shows the ratio of polymer layer per clay platelet, f_{pl}/f_C. Interestingly, this ratio is almost constant (≈2.5), regardless of C_{clay}. This value seems to be the saturated amount of PNIPA captured to clay surface.

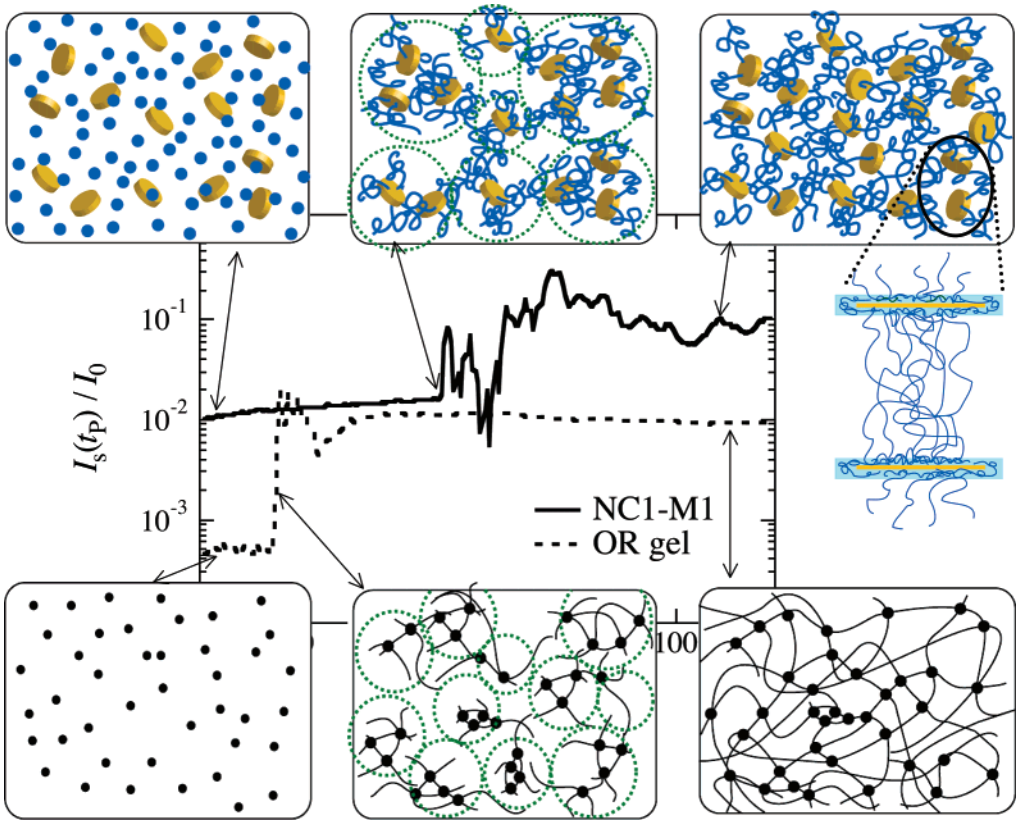

Figure 13. Scheme of the gelation mechanisms of NC gels (upper) and OR gels (lower). The middle figure is the polymerization time, t_P, dependence of the scattering intensity during polymerization. Blue dots, yellow disks, blue disks, and blue lines indicate NIPA monomer, clay platelets, polymer layers, and polymer chains, respectively.

Figure 12b shows the C_{clay} dependence of the correlation length ξ of polymer network (dashed line) and interclay distance, d_{clay} (solid line). d_{clay} is calculated by

$$d_{clay} = \left(\frac{V_C \hat{\rho}_{clay}}{m_{clay} C_{clay}}\right)^{1/3} \tag{12}$$

Here, $\hat{\rho}_{clay}$ and m_{clay} are the mass density of the clay platelet and the molecular weight of the clay platelet, respectively. The values of d_{clay} and ξ for NC gels with higher C_{clay}'s reported in the previous paper[10] are also plotted in the figure for reference, where the evaluated ξ should be similar to the value in this study. According to eq 12, d_{clay} decreases with C_{clay}. ξ seems to scale with $C_{clay}^{-1/3}$ except for $C_{clay} = 0.01$ M. Comparing ξ with d_{clay}, ξ is affected by d_{clay}. This result agrees with our previous work.[10] According to the above results, the microscopic structure of NC gels is almost the same regardless of C_{clay} except for $C_{clay} = 0.01$ M. The reason for the deviation of ξ at $C_{clay} = 0.01$ M from a straight line with the slope 1/3 is not clear at this stage.

Figure 13 summarizes gelation mechanism for NC gel schematically. The cartoons in the upper column denote time evolution of NC gels during polymerization, and those in the lower column represent that of OR gels for comparison. The middle figure is the t_P dependence of the relative scattering intensity, $I_s(t_P)/I_0$ (shown in Figure 6a). In these models, only small numbers of PNIPA chains and clay platelets are drawn for the purpose of simplicity. In the pregel solution, there exists clay platelets and NIPA monomer. As Haraguchi et al. reported,[6] initiators and catalysts are concentrated near the surface of the clay platelets. After initiation of polymerization, free radical polymerization takes place and growing polymer chains start to tie neighboring clay platelets and form finite microgel clusters. If C_{NIPA} is enough for formation of a percolated network, the size distribution of the microgel clusters becomes fractal-like at $t_P \approx t_{th}$. It follows by gel formation. This mechanism is almost the same as that of OR gels. However, as discussed above, the size of the finite clusters of NC gels near t_{th} is much larger than that of OR gels. This is why the scattering intensity at t_{th} is much larger for NC gels than for OR gels and NC gels exclusively show a sharp depression in transmittance during a course of polymerization.

Conclusion

We investigated the gelation mechanism of NC gel by DLS and contrast-variation SANS measurements. Time-resolved DLS showed similarity as well as dissimilarity of gelation mechanism between NC gels and OR gels. The contrast-variation SANS with singular value decomposition method allowed us to obtain the partial scattering functions. The following significant facts were disclosed. (1) The gelation threshold of NC gels were observed as common features of gelation, namely, an abrupt increase in the light scattering intensity, a power-law behavior in the time−intensity correlation function, and an ergode−nonergode transition. (2) The characteristic depression in optical transmittance observed exclusively in NC gels was successfully accounted for as a formation of huge clusters of NC microgels before gelation threshold. (3) There exist a polymer layer surrounding clay platelets with the thickness of ca. 10 Å irrespective of C_{clay}. (4) The correlation length, ξ, scales roughly as $C_{clay}^{-1/3}$. (5) The fraction of the polymer layer in NC gels is almost constant and is ca. 2.5 times as large as that of clay. This means that the microscopic structures of NC gels are almost the same irrespective of C_{clay}.

All of the facts support the unique structure and properties of NC gels and their significance in the mechanical properties,

such as high deformability, high toughness, high transparency, etc. It is also demonstrated that the contrast variation SANS coupled with singular value decomposition method is a powerful tool in structure investigation of multicomponent nanostructures, such as nanocomposite gels consisting of polymer, clay, and solvent.

Acknowledgment. This work was supported by Core Research for Evolutional Science and Technology (CREST), Japan Science and Technology Agency, Japan. T.K. acknowledges the support by CREST. This work was also partially supported by the Ministry of Education, Science, Sports and Culture, Japan (Grant-in-Aid for Scientific Research (A), 2006-2008, No. 18205025, and for Scientific Research on Priority Areas, 2006-2010, No. 18068004)). The SANS experiment was performed with the approval of Institute for Solid State Physics, The University of Tokyo (Proposal No. 06.237), at Japan Atomic Energy Agency, Tokai, Japan.

Appendix. Derivation of the Partial Scattering Functions for Polymer−Clay−Solvent Systems

The scattering intensity for a polymer (P)−clay (C)−solvent (S) system is given by

$$I(q) = \sum_{i=1}^{3} \rho_i^2 S_{ii} + \sum_{i<j} \rho_i \rho_j S_{ij} \tag{A1}$$

Here, ρ_i is the scattering length density of component i. By assuming incompressibility, the scattering intensity is given by

$$I(q) = (\rho_1 - \rho_3)^2 S_{11} + (\rho_2 - \rho_3)^2 S_{22} + 2(\rho_1 - \rho_3)(\rho_2 - \rho_3) S_{23} \tag{A2}$$

We rewrite the subscripts i (= 1−3) to C, P, and S, respectively. Equation A2 is equivalent to eq 3. Let us consider the scattering amplitude, $F_i(q)$, of each component, where $F_i(q)$ is related to the partial scattering function by $S_{ii}(q) = |F_i(q)|^2$. The scattering amplitude, $A_{cyl}(R,H,\beta)$, for a disk with height $2H$ and radius R, of which preferential axis is randomly oriented with respect to the z-axis with the azimuthal angle of β (see Figure 2), is given by

$$A_{cyl}(R,H,\beta) = 2V \frac{\sin(qH\cos\beta)}{qH\cos\beta} \frac{J_1(qR\sin\beta)}{qR\sin\beta} \tag{A3}$$

Hence, F_C is simply obtained by substituting $R = R_C$, $H = H_C$, and β

$$F_C = A_{cyl}(R_C,H_C,\beta) \tag{A4}$$

Next, let us obtain F_P. Here, we assume that there exists a polymer-rich layer near a clay platelet as shown in Figure 2. The volume fraction, the radius, and the height of the polymer layer are ϕ_{pl}, R_{pl}, and $2H_{pl}$, respectively. By denoting the local concentration fluctuations of polymers in the matrix being $\eta(r)$ and its volume fraction ϕ_{pn}, one obtains

$$F_P = \int_{V_c}^{V_{pl}} \phi_{pl} \exp(-i\mathbf{r}\cdot\mathbf{q})\, dV + \int \phi_{pn}\eta(r) \exp(-i\mathbf{r}\cdot\mathbf{q})\, dV - \int_{V_{pl}} \phi_{pn} \exp(-i\mathbf{r}\cdot\mathbf{q})\, dV = (\phi_{pl} - \phi_{pn}) A_{cyl}(R_{pl},H_{pl},\beta) - \phi_{pl} A_{cyl}(R_C,H_C,\beta) + \int \phi_{pn}\eta(r) \exp(-i\mathbf{r}\cdot\mathbf{q})\, dV \tag{A5}$$

Here, V_C and V_{pl} are the volume of a clay platelet and the polymer layer including a clay platelet, respectively, and the volume integration is taken over the disc specified in the equation. The partial scattering functions S_{ij} can be obtained by multiplying F_i with F_j and integrate the product over the azimuthal angle β. Hence, S_{CC}, S_{CP}, and S_{PP} are obtained as follows:

$$S_{CC} = \frac{n_C}{2}\int_{\beta=0}^{\pi} F_C^2 \sin\beta\, d\beta = \frac{n_C}{2}\int_{\beta=0}^{\pi} A_{cyl}(R_C,H_C,\beta)^2 \sin\beta\, d\beta \tag{A6}$$

$$S_{CP} = \frac{n_C}{2}\int_{\beta=0}^{\pi} F_C F_P \sin\beta\, d\beta = \frac{n_C}{2}(\phi_{pl} - \phi_{pn})\int_{\beta=0}^{\pi} A_{cyl}(R_C,H_C,\beta)\, A_{cyl}(R_{pl},H_{pl},\beta) \sin\beta\, d\beta - \frac{n_C}{2}\phi_{pl}\int_{\beta=0}^{\pi} A_{cyl}^2(R_C,H_C,\beta) \sin\beta\, d\beta \tag{A7}$$

$$S_{PP} = \frac{n_C}{2}\int_{\beta=0}^{\pi} F_P^2 \sin\beta\, d\beta = \frac{n_C}{2}\int_{\beta=0}^{\pi} \{[(\phi_{pl} - \phi_{pn})A_{cyl}(R_{pl},H_{pl},\beta) - \phi_{pl}A_{cyl}(R_C,H_C,\beta)] + \eta(q)\}^2 \sin\beta\, d\beta \approx \frac{n_C}{2}\int_{\beta=0}^{\pi} [(\phi_{pl} - \phi_{pn})A_{cyl}(R_{pl},H_{pl},\beta) - \phi_{pl}A_{cyl}(R_C,H_C,\beta)]^2 \sin\beta\, d\beta + \frac{S_{PP}^0(0)}{1 + \xi^2 q^2} \tag{A8}$$

The numerical factor $^1/_2$ in eqs A6−A8 represents the normalization factor, i.e., $\int_0^\pi \sin\beta\, d\beta = 2$, and n_C is the number density of clay platelets. In eq A8, $\eta(q)$ represents the Fourier transform of $\eta(r)$ and $S_{PP}^0(q)$ denotes the structure factor of polymer fluctuations given by Ornstein−Zernike form

$$S_{PP}^0(q) = \frac{S_{PP}^0(0)}{1 + \xi^2 q^2} \tag{A9}$$

where ξ is the correlation length. Here, we assumed that $\eta(r)$ has no cross-correlation with those of neither clay platelet nor polymer layer. As a result, the partial structure factors, i.e., eqs 6−8, of a ternary system consisting of clay, polymer, and solvent are given by eqs A6−A8.

References and Notes

(1) Schmidt, H. In *Polymer Based Molecular Composites*; Schaefer, D. W., Mark, J. E., Eds.; Materials Research Society: Pittsburgh, PA, 1990; p 3.
(2) Novak, B. M. *Adv. Mater.* **1993**, *5*, 422.
(3) Haraguchi, K.; Takehisa, T. *Adv. Mater.* **2002**, *14*, 1120−1124.
(4) Haraguchi, K.; Takehisa, T.; Fan, S. *Macromolecules* **2002**, *35*, 10162−10171.
(5) Haraguchi, K.; Farnworth, R.; Ohbayashi, A.; Takehisa, T. *Macromolecules* **2003**, *36*, 5732−5741.
(6) Haraguchi, K.; Li, H.-J.; Matsuda, K.; Takehisa, T.; Elliot, E. *Macromolecules* **2005**, *38*, 3482−3490.
(7) Haraguchi, K.; Taniguchi, S.; Takehisa, T. *ChemPhysChem* **2005**, *6*, 238−241.
(8) Shibayama, M.; Suda, J.; Karino, T.; Okabe, S.; Takehisa, T.; Haraguchi, K. *Macromolecules* **2004**, *37*, 9606−9612.
(9) Shibayama, M.; Karino, T.; Miyazaki, S.; Takehisa, T.; Haraguchi, K. *Macromolecules* **2005**, *38*, 10772−10781.
(10) Miyazaki, S.; Karino, T.; Endo, H.; Haraguchi, K.; Shibayama, M. *Macromolecules* **2006**, *39*, 8112−8120.
(11) Haraguchi, K.; Li, H.-J. *Macromolecules* **2006**, *39*, 1898−1905.
(12) Nie, J.; Du, B.; Oppermann, W. *Macromolecules* **2005**, *38*, 5729−5736.
(13) Nie, J.; Du, B.; Oppermann, W. *Macromolecules* **2004**, *37*, 6558−6564.

(14) Nie, J.; Du, B.; Oppermann, W. *J. Phys. Chem. B* **2006**, *110*, 11167−11175.
(15) Lin-Gibson, S.; Schmidt, G.; Han, C. C.; Hobbie, E. K. *J. Chem. Phys.* **2003**, *119*, 8080−8083.
(16) Lin-Gibson, S.; Kim, H.; Schmidt, G.; Han, C. C.; Kobbie, E. K. *J. Colloid Interface Sci.* **2004**, *274*, 515−525.
(17) Loizou, E.; Butler, P.; Porcar, L.; Kesselman, E.; Talmon, Y.; Dundigalla, A.; Schmidt, G. *Macromolecules* **2005**, *38*, 2047−2049.
(18) Norisuye, T.; Shibayama, M.; Nomura, S. *Polymer* **1998**, *39*, 2769−2775.
(19) Shibayama, M.; Norisuye, T.; Takeda, M. In-situ Studies on Gelation by Dynamic and Time-Resolved Light Scattering Technique. In *Polymer Network Review*; Stokke, B. T., Elgsaeter, A., Eds.; Wiley: New York, 1999; Vol. 2, pp 3−13.
(20) Norisuye, T.; Inoue, M.; Shibayama, M.; Tamaki, R.; Chujo, Y. *Macromolecules* **2000**, *33*, 900−905.
(21) Provencher, S. W. *Comput. Phys. Commun.* **1982**, *27*, 213−227.
(22) Endo, H.; Schwahn, D.; Cölfen, J. *J. Chem. Phys.* **2004**, *120*, 9410−9423.
(23) de Gennes, P. G. *Scaling Concepts in Polymer Physics;* Cornell University: Ithaca, NY, 1979.
(24) Okabe, S.; Nagao, M.; Karino, T.; Watanabe, S.; Adachi, T.; Shimizu, H.; Shibayama, M. *J. Appl. Crystallogr.* **2005**, *38*, 1035−1037.
(25) Shibayama, M.; Nagao, M.; Okabe, S.; Karino, T. *J. Phy. Soc. Jpn.* **2005**, *74*, 2728−2736.

MA070104V